Scalable methodology for the photovoltaic solar energy potential assessment based on available roof surface area: further improvements by ortho-image analysis and application

Scalable methodology for the photovoltaic solar energy potential assessment based on available roof surface area: further improvements by ortho-image analysis and application to Turin (Italy)

Luca Bergamasco, Pietro Asinari

Department of Energetics, Politecnico di Torino,
Corso Duca degli Abruzzi 24, Torino, Italy

Abstract

The ongoing rush of the UE member states to the 2020 overall targets on the national renewable energy share (see Directive 2009/28/EC), is propelling the large exploitation of the solar resource for the electricity production. However, the incentives to the large employment of PV solar modules and the relative perspective profits, are often cause of massive ground-mounted installations. These kind of installations are obviously the preferred solution by the investors for their high economic yields, but their social impact should be also considered. Over the Piedmont Region for instance, the large proliferation of *PV farms* is jeopardizing wide agricultural terrains and turistic areas, therefore the policy of the actual administration is to encourage the use of integrated systems in place of massive installations. For these reasons, an effort to demonstrate that the distributed residential generation can play a primary role in the market is mandatory. In our previous work "Scalable methodology for the photovoltaic solar energy potential assessment based on available roof surface area: application to Piedmont Region (Italy)", we already proposed a basic methodology for the evaluation of the roof-top PV system potential. However, despite the total roof surface has been computed on a given cartographical dataset, the real roof surface available for PV installations has been evaluated through the assumption of representative roofing typologies and empirical coefficients found via visual inspection of satellite images. In order to overcome this arbitrariness and refine our methodology, in the present paper we present a brand new algorithm to compute the available roof surface, based on the systematical analysis and processing of aerial georeferenced images *(ortho-images)*. The algorithm, fully developed in MATLAB®, accounts for shadow, roof surface available (bright and not), roof features (i.e. chimneys or walls) and azimuthal angle of the eventual installation. Here we apply the algorithm to the whole city of Turin, and process more than 60,000 buildings. The results achieved are finally compared with our previous work and the updated PV potential assessment is consequently discussed.

Keywords: Photovoltaic; Roof-top PV systems; Renewable Energy; GIS; Ortho-image analysis

Nomenclature

N	*Number of pixels*	[–]
S	*Roof surface*	[m^2]
R, G, B	*Color band matrices (red, green, blue)*	[–]
C, D	*Coefficient*	[–]
Ma	*Arithmetic mean (operator)*	[–]
Me	*Median*	[–]
∇	*Gradient*	[–]
i, j	*Pixel indices*	[–]
n	*Building index*	[–]
k	*Pixel region index*	[–]
ϑ	*Tilt angle*	[°]
γ	*Azimuthal angle*	[°]
λ	*Exponential distribution rate parameter*	[–]

μ	*Mean value*	[–]
σ^2	*Variance*	[–]
σ	*Standard deviation*	[–]

Abbreviations

DEM	*Digital Elevation Model*
GIS	*Geographic Information System*
RBG	*Image format*
RAM	*Random Access Memory*
HVAC	*Heating Ventil. and Air Cond. systems*

1. Introduction

As already discussed in our previous work [1], the interest on the renewable energy exploitation is growing fast in the EU member states, due to the EU directive for 2020 (Directive 2009/28/EC). In the framework of renewables, the solar energy exploitation is one of the main topics of discussion. In Italy, the national incentives to the electricity production by means of photovoltaic systems, is cause of an ongoing proliferation of *PV farms*. As regards the Piedmont region, the policy of the actual administration is to either promote solar installations and preserve agricultural and touristic areas [1]. In this perspective, the Piedmont Regional Council, and its Capital Turin in particular, are currently assuming the national leadership in the promotion and incentive of building integrated PV systems (Piedmont Regional Council [2] and [3]).

The drift to the full exploitation of integrated systems, is nevertheless hold by the lack of reliable tools to evaluate the territorial potential. Despite lots of interactive tools are by now available to compute the useful solar radiation for a given geographical area (i.e. *PVGIS Tool* [4], see also M. Šúri et al. [5] and [6]) their applications estimate the geographical potential at the detail of the urbanized areas (M. Šúri et al. [7]), which is obviously still a limit. A first tentative to address the lack of informations on the real roof surface available has been carried out by Izquierdo et al., [8], by means of a crossed sampling of various GIS and cadastral data, and by Kabir et al., [9], by the satellite image analysis. Another tentative to address the problem has been done by Wiginton et al. [10], using a specific GIS tool for the feature extraction, but they anyway make use of empirical coefficients found in literature to evaluate the availability. The importance of a reliable assessment of the roof surface available for integrated installations moreover, is not only related to the PV energy assessment, but to the full solar energy resource planning, as already proposed by Izquierdo et al. [11] for both PV and solar-thermal installations. However, as far as the authors know, there exist no tools specifically developed for a detailed roof analysis.

In the present paper we present a novel algorithm (fully developed in MATLAB®) for the systematical roof sampling, which is able to account for the roof share availability for installations, pitch brightness, shadowing and azimuthal angle of the eventual installations. Particularly, this works aims to be a methodological refinement of our previous paper [1], in which we proposed a scalable methodology for the roof-top PV system potential assessment. In that work, despite the total roof surface area has been computed on the basis of a given GIS dataset (for the entire Piedmont region), the roof surface availability has been estimated by means of cutting coefficients to take into account the shape of the roof, eventual aerials or chimneys, solar thermal installations etc. Particularly, a representative roofing typology has been assumed, and the empirical coefficients has been found via human inspection of *Google Earth*™ images. The goal of the present work is to overcome the arbitrariness of both the assumptions and the coefficients and address the computation of the real roof surface available by means of the systematical processing of geo-referenced aerial images. The present methodology is a substantial improvement in the computation of the real roof surface available, because the analysis is carried out on real aerial photographs of the geographical unit. Here we apply the methodology to the city of Turin, and process more than 60,000 buildings. The results achieved by means of the present methodology are then compared with the assumptions made in our previous work.

The outlines of the paper are as follows: the input data are first presented, together with a brief discussion on the data structure, successively the novel methodology is presented in detail together with the relative results achieved. The comparison with our previous work and a discussion of the uncertainties concludes the paper. The computational issues are presented and discussed in detail, firstly to recall the attention to the non-trivial data amount to be processed, secondly as a remark on the complete reproducibility of the methodology at different scales and for different regions.

2. Input data

2.1. Geographical metadata

The geographical and cadastral data of the Municipality of Turin, consist of a set of shapefiles *(shp)*, covering the whole extent of the City. The shapefile is a particular metadata format, thought to be used by means of a GIS software. The shapefile is basically a georeferenced layer of mathematical features, such as dots, lines or polygons. Each feature is endowed of a serie of stored attributes (see [1] for details on the format array). For the purpose of our study, we only take into account the shapefiles concerning residential and industrial buildings. The layers are organized in polygons, representing the building shapes. Each polygon is provided of its relative attributes (such as its intended use and its surface area) and the cartesian coordinates of the polygon vertices in the adopted reference system. The geo-reference system assumed for the data of the Municipality of Turin is a national reference grid: Roma40/Gauss-Boaga Time Zone 32 (Western Italy). Roma40 refers to the *Datum* of the reference system, which is the reference ellipsoid, *Gauss-Boaga* is the projection type. The current version update is September 2010.

2.2. Orthoimagery

An orthophoto, also called orthophotograph or orthoimage, is basically a high resolution aerial photograph, which has been subsequently "orthorectified". The "orthorectification" process consists in the geometrical correction of the image to achieve a uniform scale. Particularly, the main image distortion corrections are: the topografical relief distortion (using a Digital Elevation Model, DEM), the acquisition lens camera distortion and the acquisition angle. The rectified images are accurate representations of the Earth's surface and have the same scaling properties of a map, thus can be used to perform any spatial measurement and analysis (for example by a GIS software). The georeferencing system grants the correct position of the image and eventually the superimposition of other geographical data provided of the same coordinate system. The complete dataset of the Municipality of Turin, consists of 124 orthoimages [12]. Each orthoimage consists of a compressed RGB image *(jpg)* and relative reference system file, *worldfile (jgw)*, for a total data size of 2 GB ca. The acquisition years are 2002 and 2004, according to the lot (see Fig. 1 for details).

3. Data pre-processing

3.1. Image extraction

The extraction of the image of each building, passes through the superimposition of the cadastral metadata to the orthoimagery. The coherent reference systems between the two data, allow an accurate positioning of the polygons on the relative buildings in the orthoimage. A specific part of the MATLAB® code has been developed for the systematical extraction of the buildings. The code works by intersecting the two data types, according to the following steps:

1. find edges and bounding box of the selected building (Fig. 2);
2. crop the orthoimage at the bounding box (Fig. 3(a));
3. translate the polygon vertices to the cropped image pixels;
4. create a logical mask of the building (Fig. 3(b));
5. extract the building image on white background (Fig. 3(c));
6. create a new reference system file for the new image *(worldfile bpw)*;
7. save data.

The code iteratively repeats the process for all the buildings falling completelely within the selected orthoimage. In order to avoid the loss of the buildings falling on more than one orthoimage, the 124 orthoimages cannot be processed singularly, but have to be merged in a bigger mosaic. A single image of the complete extent of the city would be the excellent solution, but the data size would be (in this case) huge. The strategy adopted to tile the orthoimages and solve the problem is discussed in paragraph 3.2. The output of the code is a new uncompressed *bmp* image, the relative geo-refence system file *bpw*, and an array (*mat* file) containing all the attributes of the building. The total number of buildings of the Municipality of Turin is 61,555 for residential and 3,936 for industrial. In our analysis, we exclude from the computation those constructions catalogued as residential or industrial but not suitable for PV system installations, such as churches, barracks or bell-towers for residential and tanks or gasholders for industrial. The residential buildings to process are hence 59,861, and 3,769 the industrials, for a total number of buildings to be processed of 63,630.

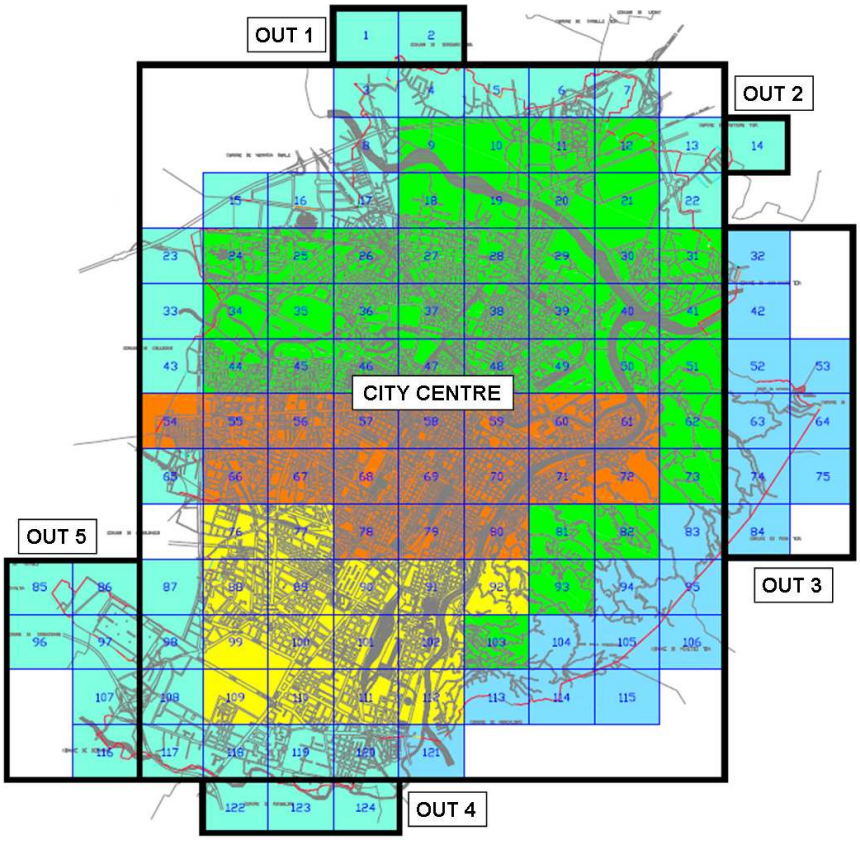

Figure 1: (color online) Overview of complete orthoimage dataset. The colors refer to the acquisition year: 2002 for lot 1 (red), 2004 for all the other lots (2 yellow, 3 green and 4 light blue). The orthoimages have been aggregated in 6 mosaics, one of the city centre and 5 of the outskirts.

3.2. Computational issues on data size

As mentioned above, the size of a single orthoimage of the entire city of Turin, would be huge. Furthermore a single image of the whole dataset would not be, in this case, an optimal solution for the reasons discussed hereafter. It should be noticed that the orthoimages are in the loosy compressed format *jpg*, and the compression rate is high and variable (5:1 or higher). In MATLAB®, the orthoimages are decompressed and stored in a 3-dimensional array, where the three matrices corresponds to the three color bands of the image: RGB (Red, Green and Blue). The original images are in the format of unsigned integer 8 bit per band (2^8 values, that is 0 to 255 colors), which means 24 bit depth color images. Despite the band matrices are in the integer format, the high compression rate of the orthoimages, causes a really high RAM (Random Access Memory) allocation. For example, a 20 MB image causes a memory allocation of 100 MB or higher, depending on the compression rate of the image. The total uncompressed data size is then 10 GB ca, but building a single image of the complete dataset in MATLAB® would lead to allocate a 3-dimensional matrix of 20 GB ca. (6.5 billion elements per band ca.) because, being the matrices square, billions of unuseful matrix elements should be anyway stored in the RAM for the background, where no data exist. Considering smaller tiles, involves anyway non-trivial computational issues, as the size of the biggest mosaic achievable directly depends on the available memory of the computer used.

The computational facility we used for the present work is the EnerGRID cluster, available at the Department of Energetics of Politecnico di Torino. It is a Transtec HPC cluster of 72 total virtual cores, 144 GB total RAM and 5.5 TB total hard disk capacity. Each node of the cluster (8 computational nodes plus the Master node), dispose of 16 GB RAM. Being the image merging a serial process (not worth to parallelize on multiple processors), we built the biggest image of the City centre compatible with the amount of memory available in one node. The dataset has been thus

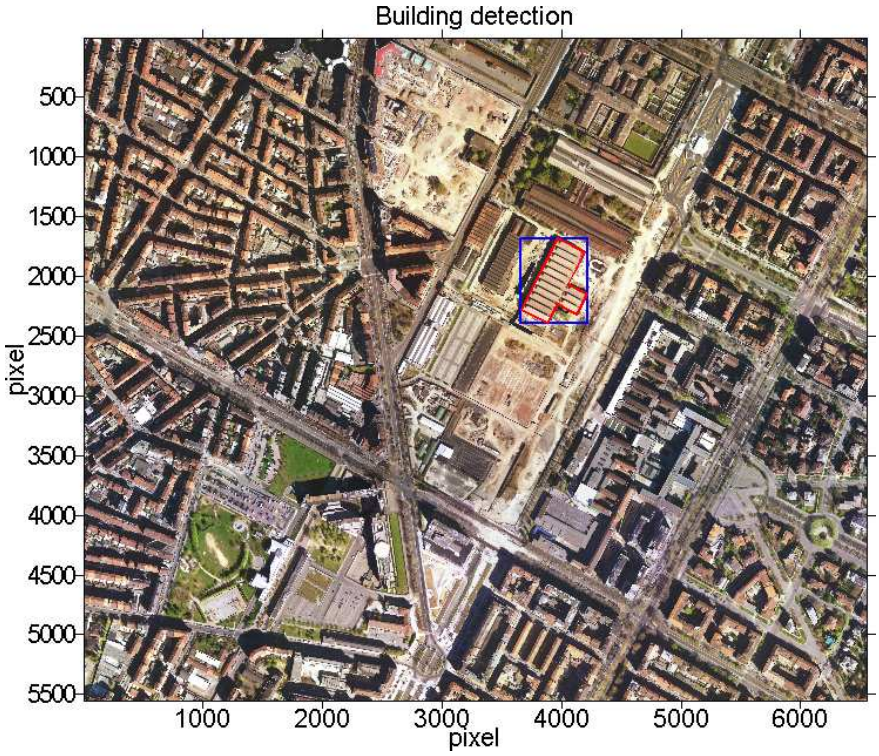

Figure 2: (color online) Building detection: the roof edges are calculated from the polygon vertex coordinates (translated to pixels). The polygon extent also allow the computation of the bounding box.

organized in a central block of 103 orthoimages for 13 GB ca (considering a 3 GB buffer for storage of variables when running code), plus 5 blocks of the outskirts (see Fig. 1). In this way, the possibility of representative data loss due to gaps among tiles is reduced to the minimum (compatibly with the computational resources), as the highest building density area is within a single block. By means of this approach, we have been able to extract 59,845 (over 59,861) residential and 3,756 (over 3,769) industrial buildings.

3.3. Data sorting and corrupted pixel identification

As already mentioned in section 2, the orthoimagery acquisition years are 2002 and 2004, while the metadata version is that of September 2010. This discrepancy between the data updates, unavoidably produces an error during the extraction of the building images. The built-up area changes in the aftermath of 2004, are indeed present in the metadata but not in the orthoimagery. The attributes of the polygons in the metadata do not provide informations about the construction year, hence it is not possible in this case to filter the selection and acquire only the buildings older than 2004 (or 2002). The algorithm inevitably extracts all the polygons, clipping also those that should be the newly built buildings. As regards the industrial case, the buildings are for the almost totality extracted properly, which means that no substantial changes have occurred for this typology after 2004. On the other hand, the residential building extraction presents a non-negligible number of fake images that must be excluded from the analysis.
Another issue concerning the building extraction is the image quality, because the extracted images present some corrupted pixel zones (Fig. 4(a)). This problem, due to the ortho-rectification algorithm (Biasion et al. [13]), is embedded in the given orthoimagery and represent a lack of informations. We decided to face the problems according to the following strategy:

1. filter the fake images;
2. identify the corrupted pixels.

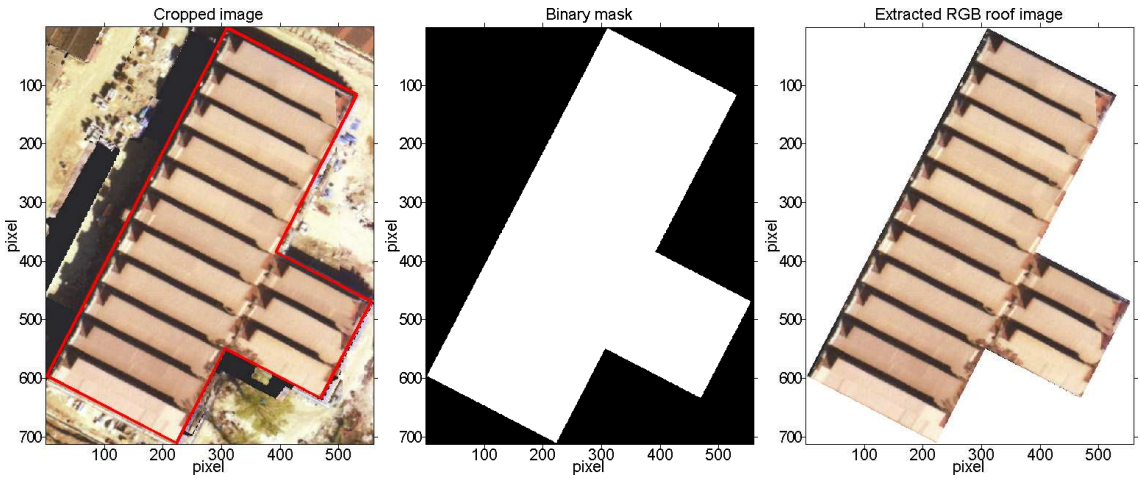

Figure 3: (color online) Building extraction process explanation: (a) roof edges and bounding box detection, (b) binary mask construction and (c) RGB roof image extraction.

As regards the first step, having no other informations, it has been decided to base the sorting algorithm on the RGB color bands. It has been found empirically that for the residential roof images, the preponderant color band is the red one. This is quite obvious for the reddish roofs, not so intuitive for the grayish. The gray color is characterised by equal values for the three color bands (RGB): at the boundaries, three zeros represent black, three 255s (in 8 bit images) represent white and all the equal terns in the middle give the different tones of gray (256 exactly). We anyway found that the grayish residential roofing present a small but significant preponderance of the red color band on the others. The imagery has been thus sorted getting rid of the images where the mean value of the blue or green color bands are greater than the red one. By means of this algorithm, the number of discarded fake "residential" images is 6,625, that is 11% of the total.

The second step, which is to identify the corrupted pixels in the images, is non-trivial, as there is no way to univocally pinpoint those pixels. They appear as variable tone dark pixels in the image, which makes it difficult to sort them as corruptions or shadows (Fig. 4(a)). We decided to make use of two crossed empirical criteria: the first based on the color darkness and the second based on the two-dimensional numerical color gradient. Particularly a pixel is defined as corruption if its color band values are all less than 50 (Fig. 5(b)) and the module of its gradient (calculated on the band with maximum variance) is greater than an imposed threshold (Fig. 5(c)). The gradient threshold is achieved evaluating the median of the color band first and then the mean of the pixels over the median. This procedure allows to evaluate the mean of the higher gradient sub-distribution only. Let the R band be that with the highest variance (could be also G or B, according to the maximum variance), the two conditions can be summarised as follows:

$$R_{ij} < 50 \qquad \textit{Condition 1}$$
$$\left|\nabla R_{ij}\right| > Ma(R_{ij} > Me(R_{ij})) \qquad \textit{Condition 2}$$

The numerical gradient of the band with maximum variance, in this case R, namely ∇R, is calculated by central finite differences with unitary step size (except at the boundaries, where forward or backward finite differences have been used).

In summary, if a pixel is dark (according to our empirical criteria, *Condition 1*) and presents a high gradient value (over the mean, *Condition 2*), then it is likely to be a corrupted pixel (i.e. very dark pixels in a coloured neighborhood). The constraint on the gradient excludes the pixels in dark clusters, because in case of clustering there is no way to univocally define a pixel as shadow or corruption. If the dark cluster is large enough, the image is excluded by the first

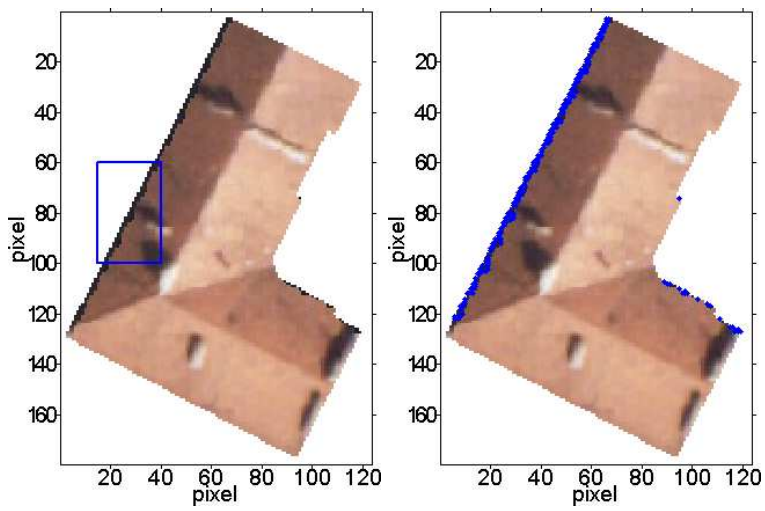

(a) (b)

Figure 4: (color online) Example roof chosen to illustrate the corrupted pixels (a). The blue box pinpoints the zoom area used in Fig. 5 to explain the algorithm developed to identify the corruptions. Identified corrupted pixels, highlighted in blue (b).

sorting algorithm based on the mean of color bands, otherwise the inner pixels of a dark cluster will be catalogued as shadow. For the sake of clarity, it must be told that we tried several ways to adjust the images and recover the corrupted pixels using filters. For example we tried to reconstruct the corruptions by interpolation of the pixel values in the local neighborhood. This method nevertheless depends on the size of the floating mask *(convolution matrix)* used to evaluate the local mean and in general produces artificial values where no data exist. We hence decided just to pinpoint and quantify the entity of the corruptions per image (excluded in the following processing) and analyse the original data (detail in Fig. 5(d) and final result in Fig. 4(b)).
It is important to remark that this part of the methodology has been specifically developed for this particular case. The sorting step has been necessary because of the discrepancy between the data updates and the fake pixel identification because of the embedded corruptions. In general, the pre-processing steps for the input data should be studied case-by-case, while the following analysis, which is the core of the proposed algorithm, applies in general.

4. Image analysis

In our previous work [1], we found the empirical coefficients used to compute the roof surface available by visual inspection of *Google Earth*™ images. The idea at the basis of the present algorithm is to translate the human-eye analysis in an computational code through statistical tools for a systematical analysis. Particularly, the purpose is to identify four zones:

- shadow;
- suitable but not bright;
- suitable and bright;
- roof features (e.g. chimneys, walls, HVAC).

Obviously we assume the shaded zones and the roof features to be not suitable for PV installations, while the suitable share is sub-divided into bright, which is recommended, and not bright, not recommended. Before proceeding, a brief clarification on this color-based division is mandatory. The analysis is carried out on aerial images, which have been acquired at a certain time of the day (and unfortunately we do not have informations on it). Rigorously, the results

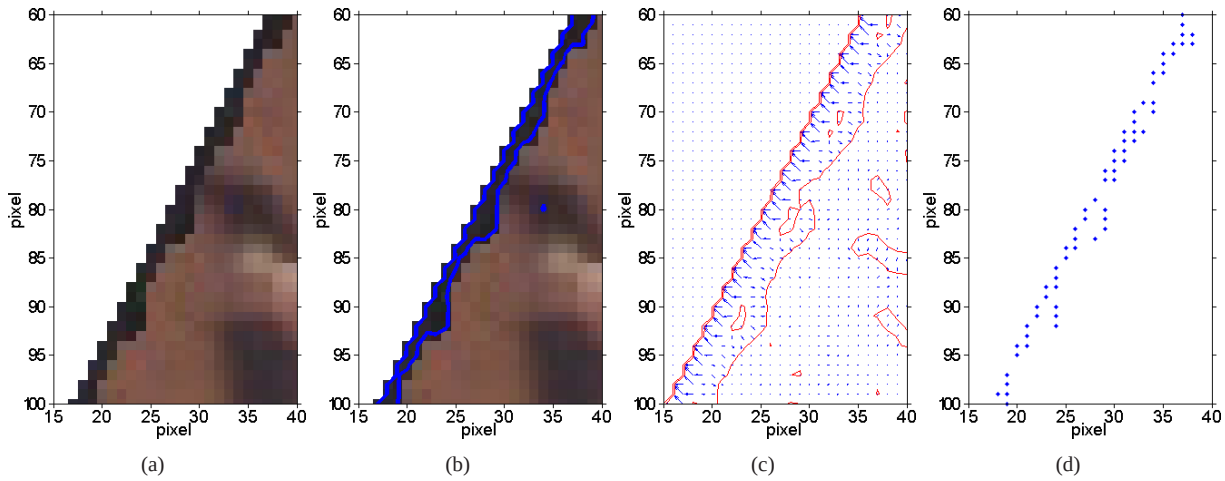

Figure 5: (color online) (a) Detail of the corrupted pixel zone (blue rectangle in Fig. 4(a)). Color isocontours for pixels characterised by all band values under 50 (b), gradient isocontours for pixels characterised by a color gradient over the threshold (c) and filtered corrupted pixels (d).

of the analysis would be therefore valid for the image acquisition time and not for all the day (neither for different periods along the year). Nevertheless, if we assume that the images are generally acquired at a good day-light time, the color-based analysis can be representative of the mean situation during the day. As regards the shadowing, for instance, its effective value should be calculated as the integral mean of the shaded zones during the day (same as for the pitch brightness). This approach however, would require a complete 3D city model or at least a complete ortho-image sample for the given geographical area acquired at different time intervals during one day. With regards to this issue, we mention a German project named SUN-AREA [14], aiming to compute the roof-top PV potential by means of aircraft scanner data. However, this method requires *ad-hoc* aerial data acquisition, while the purpose of our methodology is to provide an easy tool for the analysis of freely available and easy accessible data, therefore we assume the ortho-imagery to be representative of a mean situation during the day. This hypothesis should be always kept in mind for the algorithm steps discussed in the following paragraphs.

4.1. Dynamical image segmentation

Despite the format of the images is RGB color, for the purpose of our study we decided to perform the analysis on one of the three bands only, as the combination of the bands, in this case, does not add any appreciable additional information. The first step of the analysis is thus to identify the most significant color band to study. We then calculate the bi-dimensional variance of the three bands and assume as the most significant one that with the highest variance. On this band, we construct the pixel color histogram, with a number of bins equal to the value range of the band (one bin contains a single value). This discrete distribution can be used to dynamically found the threshold values for the image segmentation: the bin counts are indeed interpolated by a variable degree polynomial. Particularly, the thresholds should be set in correspondence to the minima of the polynomial, consequently the code adapts the degree of the polynomial in order to have at least two minima for three macro-zones (considering the boundary values). The three macro-zones are: shadow, suitable and roof features. The sub-division of the suitable zone in bright and not, is carried out considering the absolute maximum of the distribution (between the two minima). However, this division is not able to properly identify the shaded zones and the roof features, hence we doubled the number of minima to four (at least): in this way the suitable zone has been shrunk and the other two zones expanded. Hence we consider the absolute maximum as described above and the two closest minima to identify the zones. The algorithm applies both to residential (Fig. 6) and industrial (Fig. 7) roofings. Sampling the images, it has been found that two particular cases deserve a different treatment, whether the image is very bright or very dark. In this cases, the maximum of the polynomial corresponds to the last or the first stationary points respectively and there is no margin to pinpoint the features or the shadow. Hence in case of a light peak, the features are not taken into account, on the other hand in case of a dark peak the shadow is neglected. The zone thresholds are then shifted and the considered minima are those two

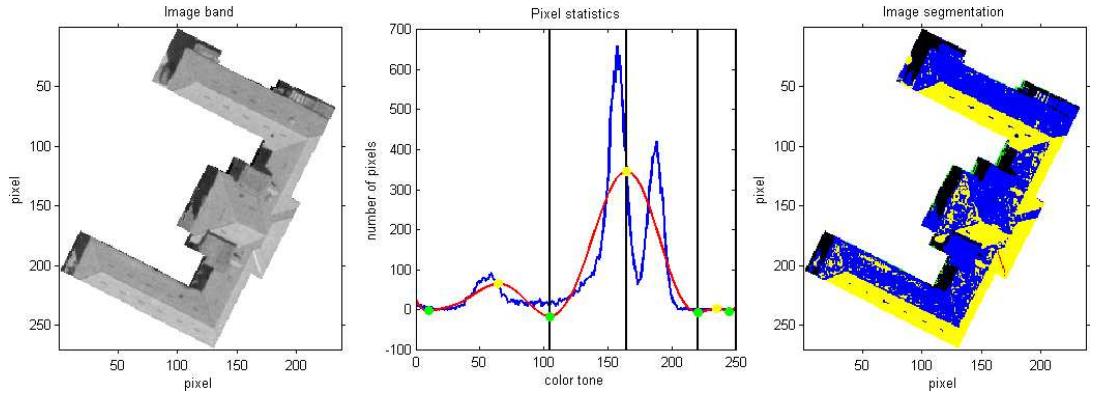

(a)

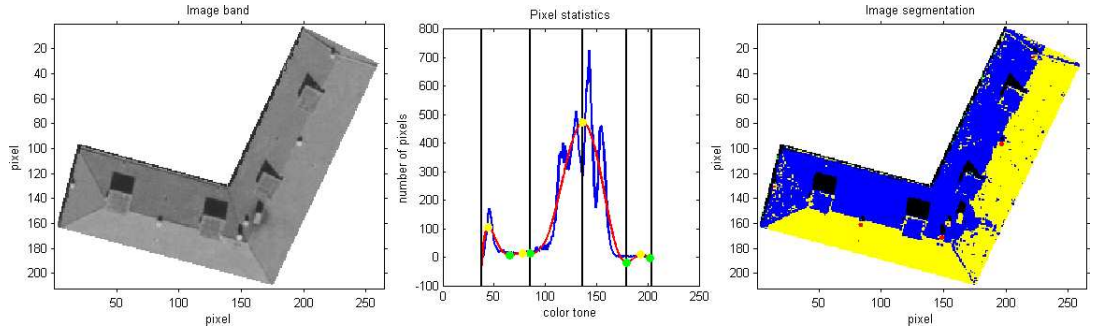

(b)

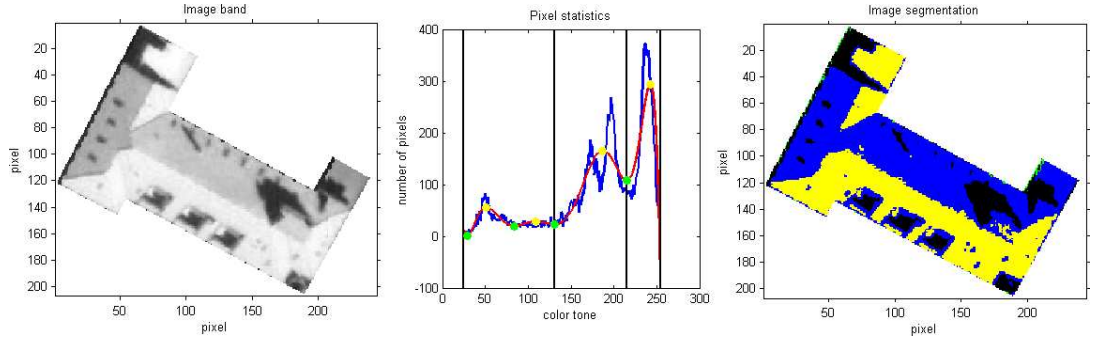

(c)

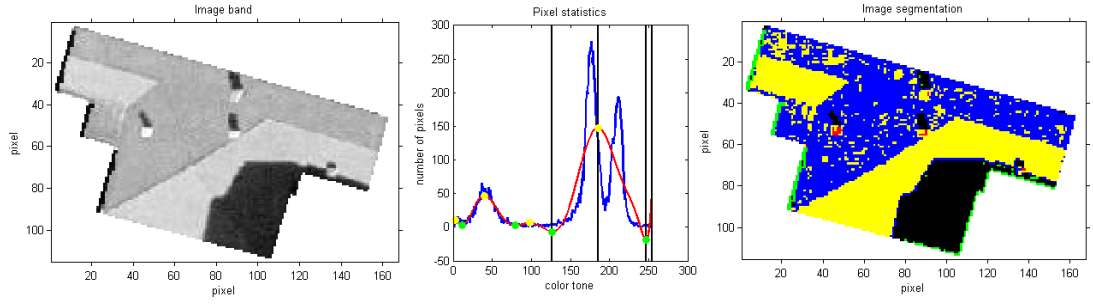

(d)

Figure 6: (color online) Residential roof segmentation. The image segmentation color legend is: green for corruptions, black for shadow, blue for suitable but not bright, yellow for suitable and bright and red for the roof features. The pixel statistics color legend is: blue for the histogram, red for the interpolating polynomial, green for the minima, yellow for the maxima and the black vertical lines are the zone thresholds.

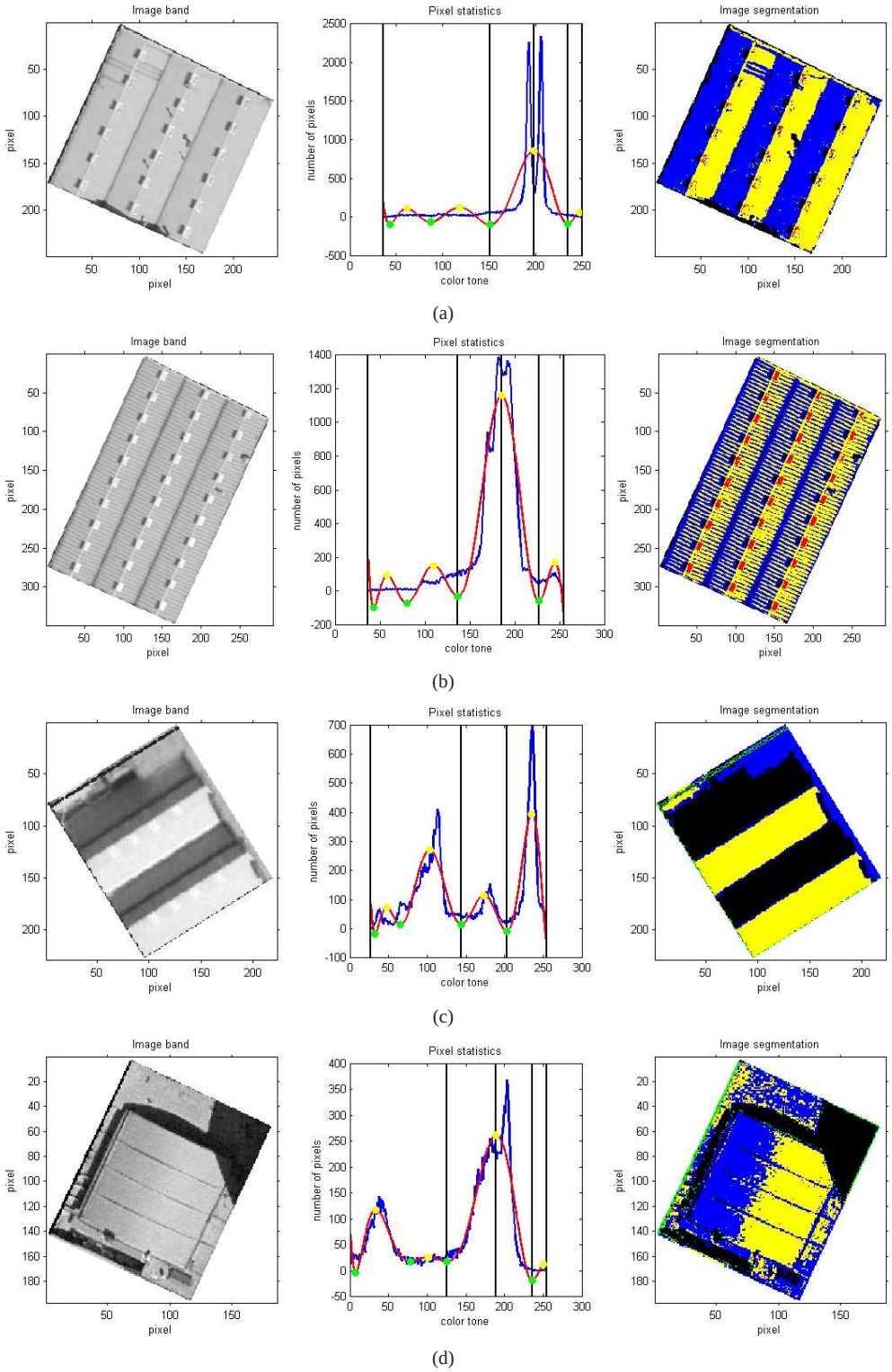

Figure 7: (color online) Industrial roof segmentation. The image segmentation color legend is: green for corruptions, black for shadow, blue for suitable but not bright, yellow for suitable and bright and red for the roof features. The pixel statistics color legend is: blue for the histogram, red for the interpolating polynomial, green for the minima, yellow for the maxima and the black vertical lines are the zone thresholds.

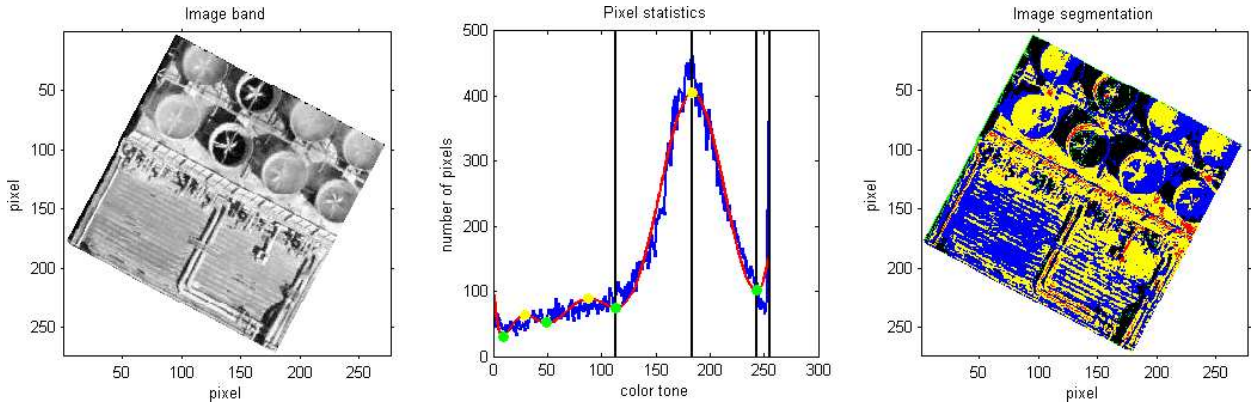

Figure 8: (color online) Particular case in which the algorithm is not able to properly identify the roof zones. The image segmentation color legend is: green for corruptions, black for shadow, blue for suitable but not bright, yellow for suitable and bright and red for the roof features. The pixel statistics color legend is: blue for the histogram, red for the interpolating polynomial, green for the minima, yellow for the maxima and the black vertical lines are the zone thresholds.

before the maximum in case of a light peak (Fig. 6(c) and 7(c)) or those two after the maximum in case of a dark peak (the maximum peak is in these cases neglected).
A last remark on the procedure is about the peak location. There exist cases where the peak is not the first or last stationary point, but it is anyway very close to the boundaries and the shadow or feature zones result to be too wide. While in these cases the shadow zone is wider than normal but reasonable (considering the strong difference between light and dark pixels), the feature zone is not, because a suitable area may result in a feature zone. We hence decided to set a constraint on the maximum share of the roof by the features, particularly we empirically found that if the biggest feature (namely, biggest cluster of pixels catalogued as features) or the total feature share exceeds 10% of the roof, then it is likely to be a wrong analysis, and we switch the zone to suitable and bright.
The accuracy of the algorithm is obviously strongly dependent on the quality of the image, if the resolution is too coarse indeed, no reliable informations can be retrieved. For this reason we decided to exclude from the sample the images with a resolution lower than 1,500 pixels, namely 9,150 residential and 197 industrial roofs. Moreover, we exclude from the sample the images characterised by a small number of color tones per band, that is the number of the histogram bins. In these cases indeed, the polynomial degree for a proper interpolation (according to the constraint on the minima discussed above) would be greater than the available data points, and the polynomial is not unique. This further exclusion leads to lower the sample to 43,503 residential and 3,558 industrial images. Finally, there exist some particular cases in which the algorithm is not able to properly identify the zones (Fig. 8), but unfortunately this is an embedded uncertainty of the color based analysis (the confidence interval of the algorithm is discussed in paragraph 6). A brief remark on the computational times: the serial processing of the residential buildings took 4 hours ca. (mean processing time per image of 0.33 s ca.) while the industrial took 1.5 hours ca. (1.5 s per image ca.).

4.2. Azimuthal angle calculation

Once achieved the suitable roof share, in order to achieve the highest conversion rate, the bright area is recommended for the PV installation. We then propose a method to evaluate the azimuthal angle of the eventual PV installations in the bright areas (γ). Being all the images endowed of their own reference system (extracted from geo-referenced datasets), the y-axis corresponds to the North-South direction and the x-axis to the West-East direction. We then calculate the orientation of the bright regions as the angle (in degrees ranging from -90 to 90 degrees) between the x-axis and the major axis of the ellipse that has the same second-moments as the region (normalized second central moments, Haralick R.M. and Shapiro L.G. [15]). A region azimuthal angle zero $\gamma = 0$ (parallel to x-axis), means south-facing PV modules (the module axis is indeed perpendicular to that of the region), the angle is then positive (γ^+) counter-clockwise and negative (γ^-) clockwise. The orientation angle is calculated for each bright region greater than 10 m^2 (that we reasonably consider the minimum significant extent for a PV system installation) and finally the weighted-average over the pixels $\gamma_{w_{mean}}$ of the obtained angles is achieved by the following equation (Eq. 1).

Figure 9: Code outcome for the residential (upper image) and industrial (lower image) roof analysis: roof share percentage of no-data, shaded share, suitable but not bright region, suitable and bright, features and weighted mean azimuthal angle of the eventual installations in the bright regions.

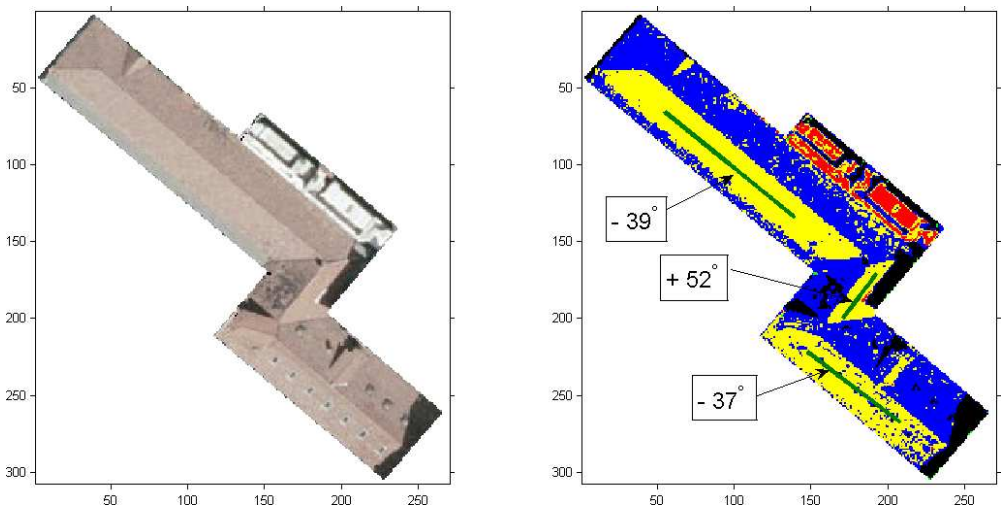

DATA	VALUE
No-data	0.1 %
Shadow	10.2 %
Suitable (not bright)	46.3 %
Suitable (bright)	39.0 %
Features	4.3 %
Weighted-mean azimuthal angle	31.5°

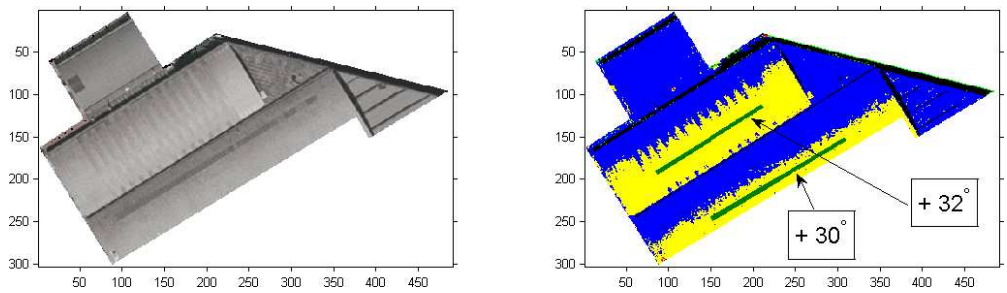

DATA	VALUE
No-data	0.7 %
Shadow	7.2 %
Suitable (not bright)	57.0 %
Suitable (bright)	35.0 %
Features	0.1 %
Weighted-mean azimuthal angle	31.5°

$$\gamma_{w_{mean}} = \frac{\gamma_1 \cdot N^{bright}_{region_1} + \ldots + \gamma_k \cdot N^{bright}_{region_k}}{\sum_k N^{bright}_{region_k}} \quad (1)$$

5. Results

The final output of the code is a detailed analysis for every single image: percentage of corrupted pixels, catalogued roof zones (shadow, suitable but not bright, suitable and bright, roof features) and weighted-mean azimuthal angle of the eventual installations in the bright regions (Fig. 9). The results achieved for the city of Turin are described in detail in the following paragraphs.

Table 1: Summary table of the results achieved (mean values) on the Municipality of Turin for the residential and industrial buildings.

DATA	RESIDENTIAL	INDUSTRIAL
No-data	1.7 %	0.8 %
Shadow	16.3 %	12.7 %
Suitable (not bright)	38.0 %	39.5 %
Suitable (bright)	43.1 %	46.0 %
Features	0.9 %	1.0 %
Weighted-mean azimuthal angle	$\approx 9°$	$\approx 7°$

5.1. Sampling of the city of Turin

After the sorting processes discussed in paragraphs 3.3 and 4.1, the image sample of the Municipality of Turin consists of 43,503 residential and 3,558 industrial buildings. The mean values of the results achieved are reported in Tab. 1, while Fig. 10 show the distributions of the results achieved on the roof segmentation for the residential (Fig. 10(a)) and industrial (Fig. 10(b)) case respectively, over the whole sample.

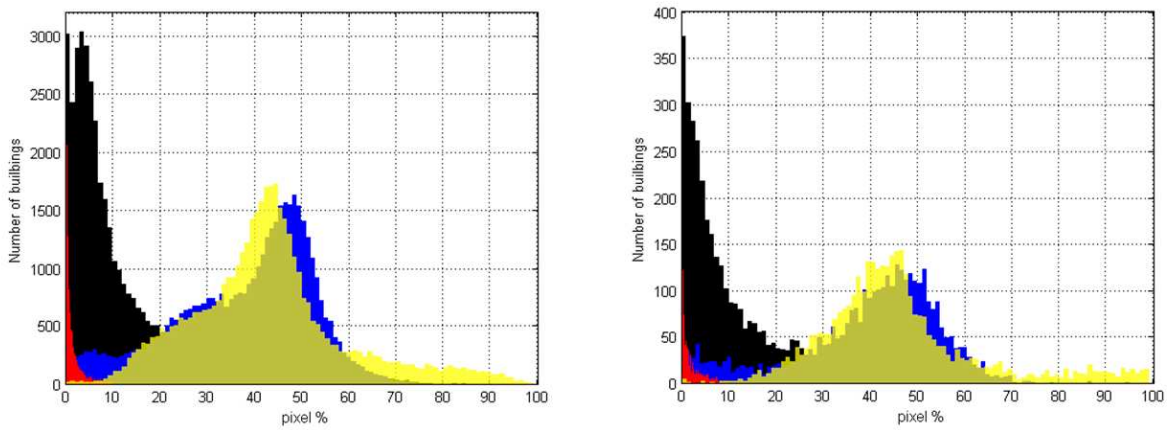

(a) (b)

Figure 10: (color online) Histogram of the roof segmentation for the residential (a) and industrial case (b) over the relative samples (43,503 and 3,558 images respectively). The color legend is: black for shadow, blue for suitable but not bright, yellow for suitable and bright and red for the roof features. Cut-off of the y-axis respectively at 3,200 and 400 (in place of 18,400 and 1,750 due to the features).

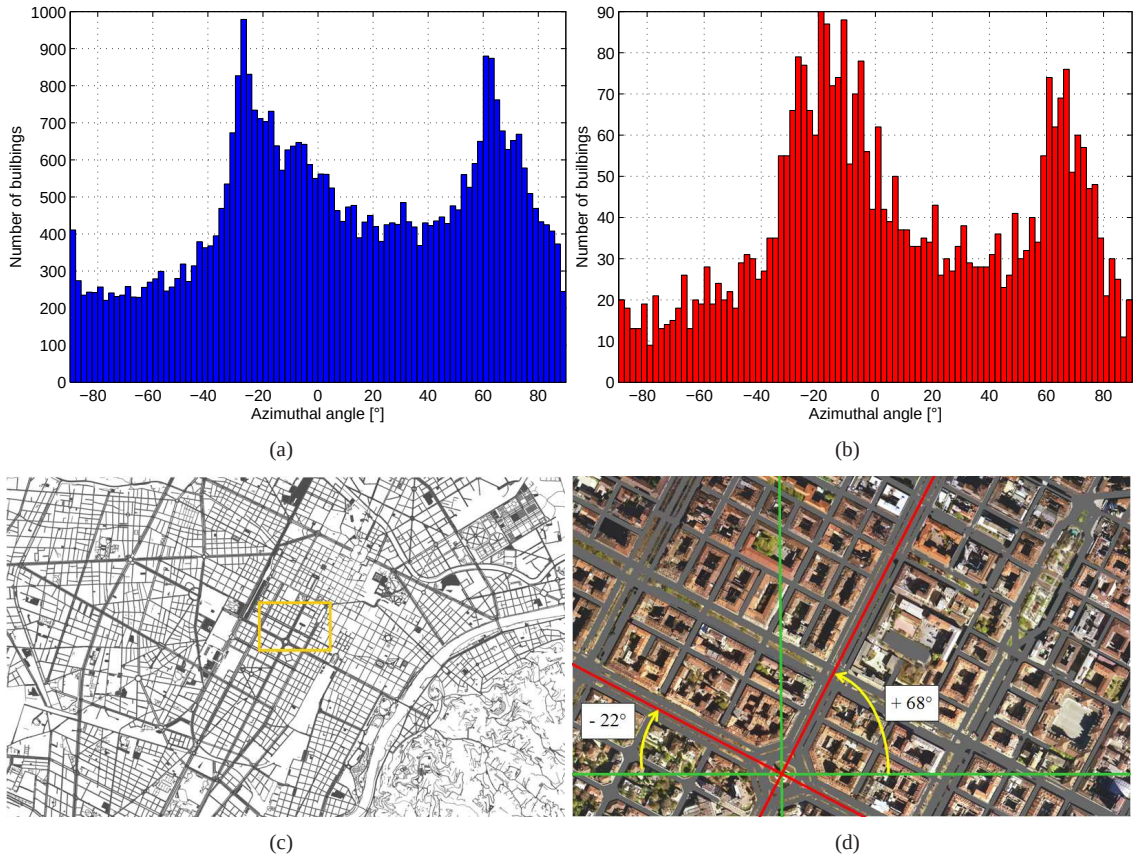

Figure 11: (color online) Histogram of the weighted-mean azimuthal angle distribution for residential (a) and industrial (b) roofs over the samples. The number of histogram bins is 90 (either cases). Street map (shapefile) of the city of Turin (c), the yellow box identifies the zoom area (d), which shows the detail of the angles of the street lattice.

The distribution of the azimuthal angles over the samples is reported in Fig. 11 (Fig. 11(a) for the residential and Fig. 11(b) for the industrial roofs). It is possible to notice that in both cases, the histograms present two distinct peaks, namely two modes. In these cases the distributions can be thought as the mixture of two (normal) distributions, characterised by different mean (μ) and variance (σ^2), namely bi-modal bi-variate distributions. As regards the comparison of the residential and industrial case, the distribution shape is consistent, particularly both cases present two modes, respectively located around -25° and 65° (Fig. 11(a) and 11(b)). If we consider that the central area of the city of Turin is characterised by perpendicular main streets and minor roads (Fig. 11(c)), an interesting conclusion can be drawn. The two modes of the azimuthal angle distributions, are located exactly in correspondence to the angles of the street lattice (Fig. 11(d)), their difference is indeed 90° ca. This result prove the reliability of the algorithm, as the weighted-mean azimuthal angles reflect the major axes of the buildings and therefore the disposition of the buildings along the streets. The shape of the cumulative distribution of the bright roof surface over the azimuthal angle for the residential case (Fig. 12(a)), is consistent with that of the histogram relative to the number of buildings over the azimuthal angle (Fig. 11(a)). Hence we are able to conclude that the bright roof surface is quite homogeneously distributed over the azimuthal angle range. On the other hand, as regards the industrial case, the shape of the cumulative distribution of the bright roof surface (Fig. 12(c)), differs significantly from the relative distribution of the number of buildings over the azimuthal angle (Fig. 11(b)). In this case, the bright roof surface is not homogeneously distributed, particularly, the highest peak in Fig. 12(c), identifies the FIAT Group Automobiles S.p.a. (the interested reader may check the consistency of the roof orientation angle of the plant facilities on *Google Earth*™). These results show that in case of a large scale analysis, it is non-trivial to figure out whether the assumption of a mean value for the azimuthal angle over the whole city can be valid or not. The correctness of this hypothesis is discussed in a dedicated paragraph,

5.2.2.

Finally, Fig. 12(b) and 12(d) show the histograms and fitted exponential distributions of the bright roof surface. For the sake of clarity, we briefly recall the definition of an exponential distribution pdf (probability density function) for a sample x (Eq. 2):

$$f(x \mid \lambda) = \frac{1}{\lambda} \cdot e^{-\frac{x}{\lambda}} \tag{2}$$

Eventually, if we consider 10 m^2 as the smallest significant extension for a solar PV installation, all the buildings disposing of a smaller bright area (namely contiguous bright pixels) should be excluded from the suitable. Considering a 10 m^2 cut-off, would lead to exclude almost 4,500 residential (Fig. 12(b)) and more than 150 industrial (Fig. 12(d)) buildings (that is respectively 10% and 4% ca. of the samples).

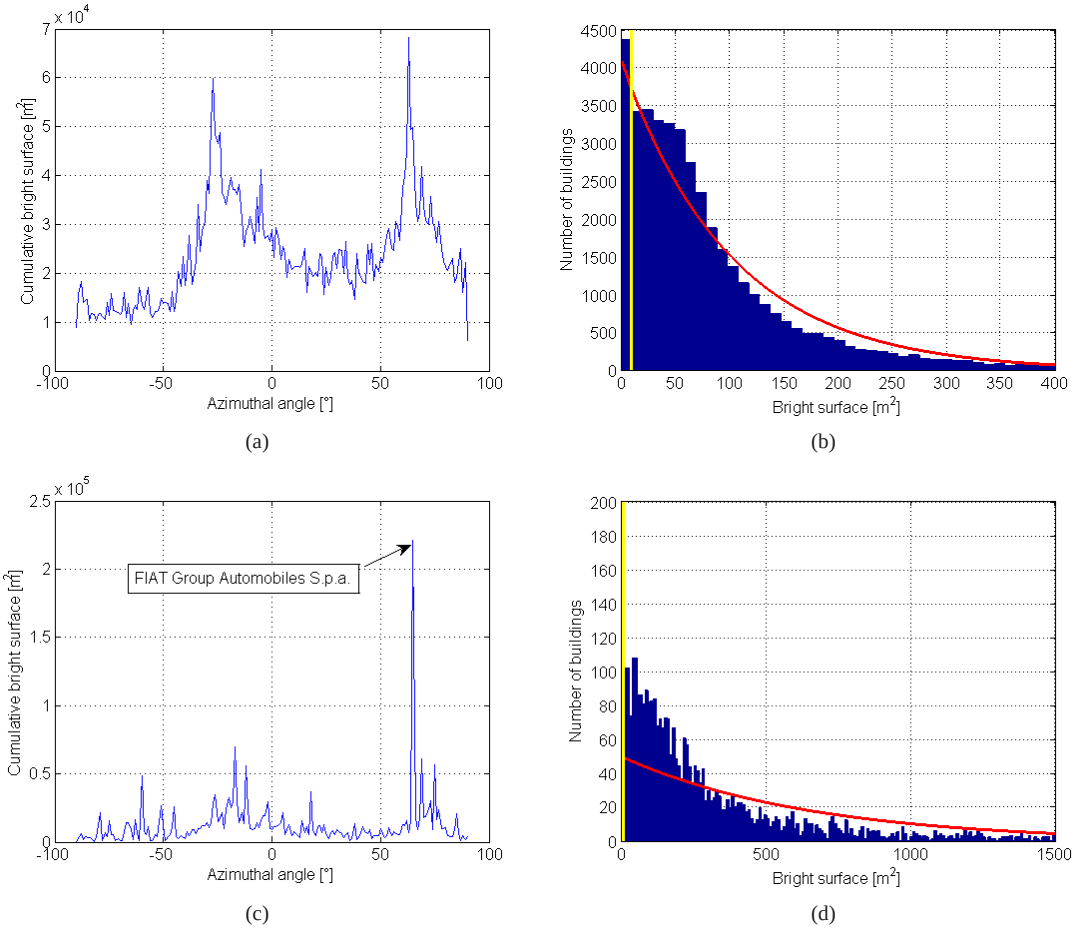

Figure 12: (color online) Cumulative bright roof surface [m^2] over the azimuthal angle for the residential (a) and industrial (c) cases. Histogram (blue) and fitted exponential distribution (red) of the bright roof surface, (b) residential and (d) industrial. Number of bins respectively 2,500 and 21,348. The cut-off point (yellow) is 10 m^2 in both cases. The cut-off of the axes are: (b) y-axis 4,500 and 400 x-axis, (d) y-axis 200 and 1,500 x-axis. Exponential distribution rate parameters: λ_{res} = 101 m^2, λ_{ind} = 649 m^2. Remark: the industrial exponential distribution appears to be badly fitted, this is due to the axis cut-off to allow a proper visualisation.

5.2. Comparisons with our previous work

In this paragraph, the results achieved by the presented methodology for the city of Turin are compared with those in our previous work, [1]). Sub-paragraph 5.2.1 deals with the discussion of the previously assumed and newly computed

coefficients to achieve the roof surface available. The effect of the resulting error on the roof-top PV potential for the city of Turin is also discussed. In sub-paragraph 5.2.2, the previously assumed mean coefficient for the azimuthal angle loss (*azimuthal efficiency* η_{AZ}) is compared to the weighted-mean values over the two samples (residential and industrial) achieved by the present methodology.

5.2.1. Roof-top PV potential

As already discussed, in our previous paper [1], the roof surface available has been computed by means of empirical coefficients found via visual inspection of satellite images. Particularly, the introduced cutting coefficients were: a *shadowing coefficient* C_{SH} for the shadowing, a *roof-type coefficient* C_{RT} for the shape of the roof, a *feature coefficient* C_F and a *solar-thermal coefficient* C_{ST} for the already occupied roof surface due to chimneys, aerials or solar-thermal installations. The available roof area has been consequently computed by product of the coefficients, namely (Eq. 3):

$$S_{avail} = S_{roof} \cdot C_{SH} \cdot C_{RT} \cdot C_F \cdot C_{ST} \tag{3}$$

This approach has been largely used in literature (see for instance, Izquierdo et al. [8]), as it is mandatory when the roof exploitability is unknown. This method however, may result to be too conservative, as the product progressively cut the same surface (and this is even statistically unlikely). In the present work, under the hypothesis discussed in paragraph 4, that is, the results achieved on the ortho-imagery represent a mean situation during the day (in place of integral mean values), the algorithm yields directly the effective available bright roof share. Eventually, considering the newly computed roof partitions, the bright area can be achieved by subtraction of the non-suitable zones to the total roof surface. Particularly, in analogy with our previous work, the mean values in Tab. 1 (divided by 100) can be defined as a new set of cutting coefficients: no-data D_{ND}, shadow D_{SH}, suitable (not bright) D_{RT} and features D_F. The mathematical definition of the new cutting coefficients however, is radically different between the two papers, therefore in this case the suitable area is calculated by means of Eq. 4, namely:

$$S_{avail} = S_{roof} \cdot (1 - (D_{ND} + D_{SH} + D_{RT} + D_F)) \tag{4}$$

The comparison between Eq. 3 and 4, allows to understand the methodological difference of the two approaches. As regards the representative roof inclination angles (ϑ_{RES} and ϑ_{IND}), we still make use of our previously assumed values [1], namely 20° for ϑ_{RES} and 30° for ϑ_{IND}. Assuming representative values for this characteristic is still the only way to take into account the 3D roof topology and correct the computed planary surfaces, because the orthoimagery does not allow the retrieval of the 3D roof shape. Considering a sufficient spacing between modules to avoid reciprocal shadowing, namely our previously assumed value for the *covering index coefficient* $C_{COV} = 0.45$ [1], according to the present methodology, the available roof surface area for the Municipality of Turin may be 41% higher than that computed in our previous work. The total PV potential for the three scenarios (A, B and C) presented in our previous work, would hence be respectively 719, 858 and 343 $GWh/year$.

5.2.2. Azimuthal angle

In our previous work [1], we assumed a mean azimuthal angle loss, *azimuthal efficiency* $\eta_{AZ} = 0.9$ over the Piedmont Region, (UNI 10349 [16] and UNI 8477/1 [17]). This value can be easily obtained by regression using the interactive web tool *Atlante Italiano della radiazione solare*, of the Italian National Agency for New Technologies, Energy and Sustainable Economic Development (ENEA, [18]), which is indeed based on this regulation. For the sake of completeness, we compared this result with that obtained by another interactive web tool, the *PVGIS* tool, [4]. In both cases, in a set condition, the value of the azimuthal angle has been made varying from 0 to 90, and the calculated outputs have been used to evaluate the influence of the azimuthal angle on the output. For the municipality of Turin, the first tool yields exaclty $\eta_{AZ} = 0.9408$ and the second $\eta_{AZ} = 0.9243$. Interpolating the values obtained by regression on the outputs of the two web tools (Fig. 13), it is possible to calculate the azimuthal angle loss as a function of the azimuth γ, namely for each single roof $\eta_{AZ}(\gamma)$.

$$\eta_{AZ_{mean}} \stackrel{?}{=} \frac{\sum \eta_{AZ}(\gamma_n) \cdot S_n^{bright}}{\sum S_n^{bright}} \tag{5}$$

The comparison of the mean values with the relative weighted-mean on the bright roof surface (Eq. 5) allows to verify wheter the assumption of the a mean value for a large scale analysis can be valid or not (hypothesis discussed in

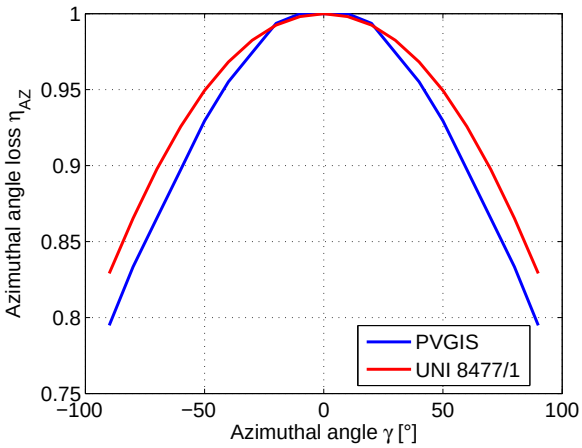

Figure 13: (color online) Azimuthal angle loss (η_{AZ}) as a function of the azimuthal angle (γ). Comparison of the curves obtained by regression on the two web tools: *PVGIS* tool, [4] and *Atlante Italiano della radiazione solare*, [18].

paragraph 5.1). The weighted-mean based on the regression on the first tool yields $\eta_{AZ} = 0.9381$ instead of the mean value $\eta_{AZ} = 0.9408$, while the PVGIS data yields $\eta_{AZ} = 0.9190$ in place of $\eta_{AZ} = 0.9243$. The negligible difference of the comparisons allows to conclude that for the large scale analysis, the assumption of a mean value for the azimuthal angle loss is consistent (at least for the city of Turin). However, in case of a detailed analysis, the algorithm output provides anyway the possibility to evaluate the loss due to azimuth at the detail of the single bright zone for each roof.

6. Confidence level

In this paragraph the uncertainties affecting the proposed methodology and the reliability of the algorithm are discussed. The first limit to consider is the image resolution, the pixel is the smallest significant unit to consider (despite interpolation) and no useful informations can be retrieved beyond it. Therefore any detail smaller than the pixel size, cannot be identified (i.e. thin aerials).
The second cause of uncertainty to consider is the error due to the building image extraction. The roof images indeed, have been extracted using the polygons of the geographical metadata to clip the ortho-imagery. Despite the consistency of scales and geo-reference systems between the data allow the correct position and overlay, the intersection between the polygon edges and the underlying pixels produces an approximation during the clipping, because of the pixel size (sort of *pixelation* of the edges). The surface of the extracted images indeed, do not exactly correspond to that declared in the attributes stored in the metadata. This error is anyway negligible, as its mean value over the whole sample analysed is 0.1%.
The core of the analysis of the uncertainties, is to evaluate the reliability of the proposed methodology and provide a confidence interval on the quality of the analysis. We then propose an empirical method to quantify the error made on the roof segmentation. The algorithm output is visually analysed for a sample of 250 residential and 250 industrial buildings and a mark (from 5 to 10) is given to the quality of the analysis. A 10 mark, for instance, corresponds to the 100% accuracy of the analysis (i.e. feature identification, identified corruptions, etc.), while a 8 mark denotes an accuracy error of 20% on the overall result (according to the human visual inspection). Obviously, the quality of the analysis reflects the quality of the given image: if the quality is poor, the analysis is not reliable. In these cases however, if the algorithm works as it is expected to do, a good mark is given (as even the human-eye is not able to properly identify the roof zones). Low marks are given if the original image is clear but the algorithm is not able to properly identify the roof partitioning. On the basis of this preliminary remarks, the results of the quality evaluation show a mean accuracy level around 90% for the two samples examined.
This empirical approach to the evaluation of the correctness of the analysis is clearly affected by an embedded uncertainty due to the human sensibility. Nevertheless, this procedure represents a first tentative to address the non-trivial

problem of the error estimation. A real validation indeed may be achieved only by comparing the results of the analysis against real data (i.e. monitored integrated PV systems) and at today, we do not dispose of this kind of data for the city of Turin. The opportunity for a validation may come from the application of the algorithm to a territory where real data exists.

7. Conclusions and perspectives

In the present work, a novel approach to compute the available roof surface for solar integrated installations has been proposed. The presented methodology accounts for the roof surface available for installations, roof typology (through the analysis of the brightness), shadowing, already occupied roof surface and azimuthal angle of the eventual installations. The presented algorithm has been applied to the whole city of Turin, and the results achieved on the roof exploitability and on the relative roof-top PV potential have been compared with those obtained in our previous work, [1]. Mostly due to the different approaches in the evaluation of the bright roof surface, the comparison has shown that in our previous work the assessment has been largely conservative. According to the present methodology indeed, the total roof-top PV potential for the municipality of Turin may be 41% higher.
The reliability of the methodology has been proved comparing the outcomes on the azimuthal angles of the bright areas with the street topology of the city, and a confidence interval has been given to the accuracy of the algorithm (around 90%, according to the human visual inspection).
As a concrete application of the presented methodology, the authors would like to mention that the results achieved in the present paper have been aggregated to the official cartographical metadata *(shapefiles)* of the Municipality of Turin. By means of a GIS sofware, even an unskilled user, can now interactively interrogate each building and view the informations about the roof exploitability. The authors are also actively working on the source code for the development of an automatic web plug-in for a real-time analysis.
As regards the methodological perspectives instead, despite the presented algorithm represents a step forward in the evaluation of the roof surface available for integrated solar installations, the computation of the real (mean-time-integral) shadowing and roof brightness still remains an open issue. The in-time analysis would require indeed a complete 3D city model (and an artificial-sky model) and, at today, we do not dispose of data at this detail for the city of Turin.

Acknowledgments

We are grateful to Regione Piemonte for the financial support of the present work through the EnerGRID project. Thanks to Altair Engineering, industrial partner of the project, in particular Paolo Masera is kindly acknowledged. Thanks to Gianfranco Pirrello, of the City of Turin Council, Settore Gestione Informatica Divisionale e Banche Dati D.I.A.N.A., for the cartographical data. The authors would also like to sincerely thank Dr. Danilo Godone for his time and willingness, in particular for his hints on the cartographical data.

References

[1] Bergamasco L., Asinari P., *Scalable methodology for the photovoltaic solar energy potential assessment based on available roof surface area: application to Piedmont Region (Italy)*, Solar Energy (accepted with minor revisions).
[2] Regional Council of Piedmont, energy and environment section. 2011, (www.regione.piemonte.it/ambiente/energia/home.htm).
[3] Regional Council of Piedmont, renewables section. 2011, (www.regione.piemonte.it/energia).
[4] JRC, 2011. Joint Research Centre of the European Commission, IE Institute for Energy. *PVGIS*, (http://re.jrc.ec.europa.eu/pvgis/).
[5] Šúri M., Dunlop E. D., Huld T. A., 2005. *PV-GIS: A web based solar radiation database for the calculation of PV potential in Europe*, International Journal of Sustainable Energy 24 (2), 55-67.
[6] Šúri M., Huld T., Cebecauer T., Dunlop E.D., *Geographic Aspects of Photovoltaics in Europe: Contribution of the PVGIS Website*, IEEE Journal of Selected Topics in Applied Earth Observations and Remote Sensing, v 1, n 1, p 34-41, 2008.
[7] Šúri M., Huld T., Cebecauer T., Dunlop E.D., Ossenbrink H.A., *Potential of solar electricity generation in the European Union member states and candidate countries*, Solar Energy 81 (2007) 1295-1305.
[8] Izquierdo S., Rodrigues M, Fueyo N., *A method for estimating the geographical distribution of the available roof surface area for large-scale photovoltaic energy-potential evaluations*, Solar Energy 82 (2008) 929-39.
[9] Kabir, Md.H., Endlicher, W., Jgermeyr, J., *Calculation of bright roof-tops for solar PV applications in Dhaka Megacity, Bangladesh*, Renewable Energy 35 (8) (2010), pp. 1760-1764.
[10] Wiginton, L.K., Nguyen, H.T., Pearce, J.M., *Quantifying rooftop solar photovoltaic potential for regional renewable energy policy*, Computers, Environment and Urban Systems 34 (4) (2010), pp. 345-357.

[11] Izquierdo S., Montanés C., Dopazo C., Fueyo N., *Roof-top solar energy potential under performance-based building energy codes: The case of Spain*, Solar Energy 85 (2011) 208-213.
[12] Municipality of Turin Council, Settore Gestione Informatica Divisionale e Banche Dati D.I.A.N.A. (Cartographical Department), 2010.
[13] Biasion A., Dequal S., Lingua A., *A new procedure for the automatic production of true orthophotos*, ISPRS XXth congress proceedings, ISPRS XXth congress, Istanbul 12-23/07/2004, 2004.
[14] SUN-AREA Research Project, http://www.sun-area.net/, 2011.
[15] Haralick R.M., Shapiro L.G., *Computer and Robot Vision*, vol. I Appendix A, Addison-Wesley, 1992.
[16] UNI 10349, 1994.
[17] UNI 8477/1, 1983.
[18] Italian National Agency for New Technologies, Energy and Sustainable Economic Development, 2011. *Atlante Italiano della radiazione solare*, (http://www.solaritaly.enea.it/CalcComune/Calcola.php).